J Nanostruct 16(1): 625-636, Winter 2026

RESEARCH PAPER

Comparative Study of the Structural, Electrical, and Antibacterial Properties of ZnO, NiO, Fe_2O_3 Oxides Prepared by Pulsed Laser Deposition Technique

Huda Musa Mutlaq *, Ahmed K. Abbas

College of Sciences, Wasit University, Wasit, Iraq

ARTICLE INFO

Article History:
Received 05 October 2025
Accepted 26 December 2025
Published 01 January 2026

Keywords:
Antibacterial activity
Conductivity properties
Fe_2O_3
PLD
Thin films
ZnO

ABSTRACT

The ZnO, NiO and Fe_2O_3 oxides were deposited as thin films by pulsed laser deposition (PLD) at two energy densities (500 and 700 mJ). Therefore, the purpose of the work was to investigate the effects of processing energy on the structural, morphological, electrical and biological properties of the obtained films. X-ray diffraction (XRD) measurements confirmed that pure crystalline phases were obtained in all the samples (i.e. a wurtzite phase for ZnO, a rock-salt phase for NiO, and a hematite phase for Fe_2O_3). Crystallinity and grain size developed with increasing energy except NiO which showed abnormal behavior due to internal stresses. Field-Emission scanning electron microscopy (FE-SEM) demonstrated that the particles were mostly spherical and the size was controlled by the processing energy. Particle size was found to increase for ZnO and NiO while it was decreased for Fe_2O_3 when 700-mJ energy density was used, which can be attributed to an increased nucleation rate. Electrical measurements showed the films to be semiconducting in nature, and the conductivity was increased by post-deposition heating. The maximum conductivity was obtained for the samples which were prepared at 700 mJ, which was associated with higher crystallinity and lower structural defects. The conductivity was found to be in the following order: NiO, Fe_2O_3, ZnO. Metabolite bioactivities revealed obvious inhibition against Escherichia coli and Staphylococcus aureus, in which the inhibition strength increased with increasing energy density and concentration. ZnO showed the highest antibacterial activity with an inhibition zone of 32 mm against S. aureus followed by Fe_2O_3 and then NiO. These results highlight the important role that the surface structure plays in improving the biological performance of the thin films.

How to cite this article
Mutlaq H., Abbas A. Comparative Study of the Structural, Electrical, and Antibacterial Properties of ZnO, NiO, Fe_2O_3 Oxides Prepared by Pulsed Laser Deposition Technique. J Nanostruct, 2026; 16(1):625-636. DOI: 10.22052/JNS.2026.01.056

INTRODUCTION

Over the past decades, the pulse laser deposition (PLD) has become particularly relevant as one of the most sophisticated ways of creating high purity nanostructured films and oxides. This method is characterized by the evaporation of a solid target by laser pulses of high-energy in the prepared medium to allow homogeneous sub layers to be deposited with strictly determined crystalline structure and thickness to be used

* *Corresponding Author Email: 1 hudamusa@uowasit.edu.iq*

[1,2]. This method has been employed with much success to synthesize transition metal oxides (including zinc oxide, nickel oxide, and iron oxide) because of their characteristic properties, including: wide band gap, optical activity, and chemical stability since the 1990s [3,4]. One of the most valuable semiconductor oxides (3.3 eV band gap) is zinc oxide and it has found applications in sensing, photonics and in solar cell applications [5,6]. Nickel oxide is one of the P-type semiconductor being magnetic in nature with high bactericidal capacity at nanometer scale which is applicable in electrodes and gas sensors. In the meantime, iron oxide (hematite) has outstanding photo catalytic and electrochemical activity, as well as, anti-bacterial growth activity due to the production of reactive oxygen species (ROS). PDL method enables the optimization of structural and electrical characteristics of these oxides through the control of the laser intensity, the oxygen pressure, and the temperature of substrate hence enhancing both the conductive characteristics and antibacterial actions on a functional basis. The recent reports have indicated that zinc oxide, nickel oxide and iron oxide films synthesized by this method exhibited regular crystal structure, increased conductivity as well as high chemical stability that make them potential application prospects in sensors, optical devices, or biomedicine [7,8]. The importance of this study is that, three metal oxide nanostructures, i.e., NiO, ZnO, and Fe_2O_3, were prepared and characterized via pulsed laser deposition (PLD) technology, which is a sophisticated and efficient method to prepare a quality film of different materials. This technique helps in enhancing the structural and surface properties of the films making them more suitable to be used in industrial and medical applications. Moreover, the correlation of these films in structure and electrical properties to their antimicrobial activity gives a fresh insight on the application of such films in bioelectronics devices and antimicrobial materials, and the creation of medical applications on the basis of nanotechnology [9,10].

MATERIALS AND METHODS

Laser Deposition Method for Thin Films

Thin films of ZnO, NiO, and Fe_2O_3 were deposited on glass substrates using a pulsed laser deposition (PLD) system with Nd-YAG laser (1064 nm, 6 Hz). High-purity metal targets of (Zinc oxide, Nickel oxide and Iron oxide) were used laser ablation was performed in an Oxygen atmosphere at pressure of 2.5×10^{-3} mbar. Laser energy ranged from 500 to 700 mJ. The optimum deposition time was

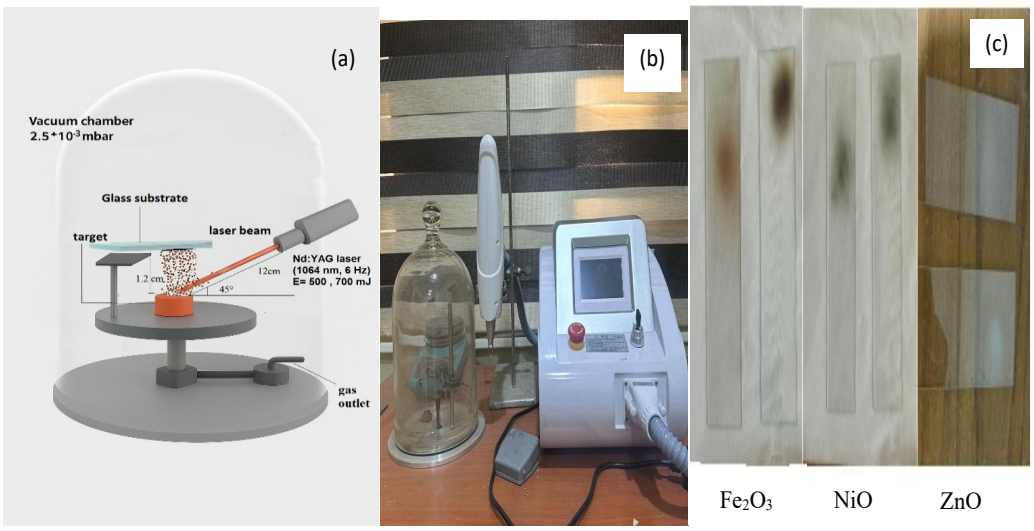

Fig. 1. Illustrates the process of deposition of thin films of metal oxides using pulsed laser deposition (PLD). (a) Schematic representation of the PLD system showing the system components and the laser path in the vacuum chamber. (b) Actual image of the PLD system used for deposition of thin films in the laboratory. (c) Image of glass samples after the deposition process with layers of (ZnO), (NiO) and (Fe_2O_3) deposited on their surfaces.

determined to achieve a film thickness of about 200 nm. Note the shape and layout of the system with photos of the samples after deposition (Fig. 1).

RESULTS AND DISCUSSION

X-ray Diffraction (XRD)

X-ray diffraction analysis was performed to study the crystal structure of the samples prepared using pulsed laser deposition (PLD). This analysis aimed to identify the crystal phases and evaluate the crystallinity and purity of the samples. The XRD patterns of NiO samples prepared by PLD at 500 and 700 mJ show that all peaks correspond to the cubic (rocksalt) structure of NiO (see Fig. 2). The peaks at 700 mJ exhibit higher intensity and narrower width, particularly for the (111) and (200) planes, indicating improved crystallinity and larger crystallite size in these directions. In contrast, the (220) and (311) peaks show broader widths and smaller calculated crystallite sizes, suggesting anisotropic growth or internal stress. The crystallite size values were calculated using the Scherrer equation ($D=K\lambda/(\beta \cos\theta)$), which depends on the full width at half maximum (FWHM) of the peak and the diffraction angle, and provides an estimate of the average crystallite size along the specific plane. Overall, the average

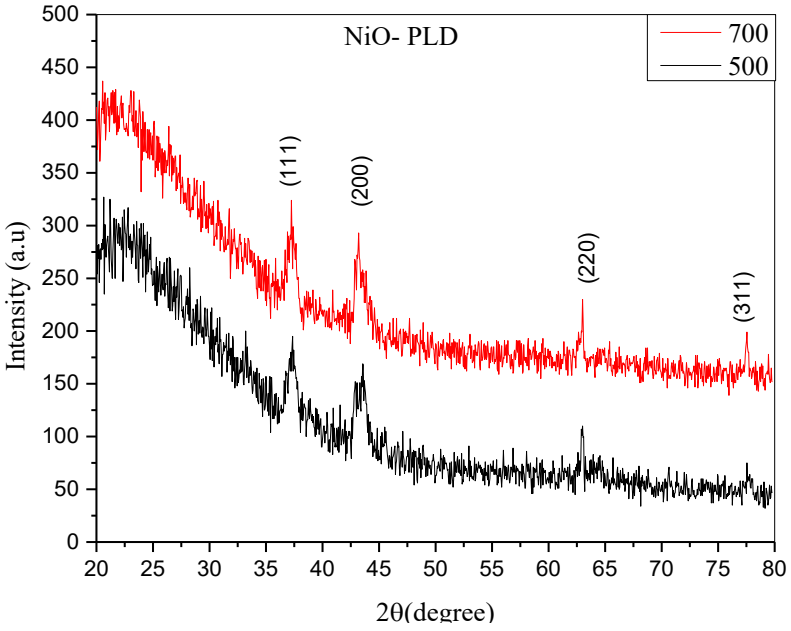

Fig. 2. XRD pattern of NiO nanoparticles PLD.

Table 1. XRD data of NiO nanoparticles PLD.

energy	hkl	2θ (Deg.)	FWHM (Deg.)	dhkl Exp.(Å)	C.S (nm)
500	111	37.30	1.87	2.41	4.48
	200	43.67	1.42	2.07	6.03
	220	62.98	0.31	1.47	30.05
	311	77.68	0.33	1.23	30.91
700	111	37.20	1.29	2.42	6.47
	200	43.12	1.28	2.10	6.67
	220	62.98	0.49	1.47	19.01
	311	77.46	0.36	1.23	28.29

crystallite size decreased from approximately 17.9 nm at 500 mJ to approximately 15.1 nm at 700 mJ (Table 1). This change is attributed to the higher laser energy, which increases particle energy and surface mobility, improving crystallinity in some directions, but may also introduce defects or internal stress, leading to smaller crystallite sizes in other directions. This is consistent with previous literature, which also suggests the possibility of anisotropic crystal growth or preferred crystallographic orientation [11, 19, 20].

The X-ray diffraction (XRD) results for the zinc oxide samples prepared using the PLD technique at two different laser energies (500 and 700 mJ) (see Fig. 3) showed distinct diffraction peaks at the (100), (002), (101), (102), (110), (103), and (112) planes, corresponding to the hexagonal (wurtzite) structure of ZnO. The peaks at 700 mJ were sharper and more intense, indicating improved crystallinity and larger crystallite size, while the peaks at 500 mJ were broader and less intense, reflecting a smaller crystallite size and lower crystallinity.

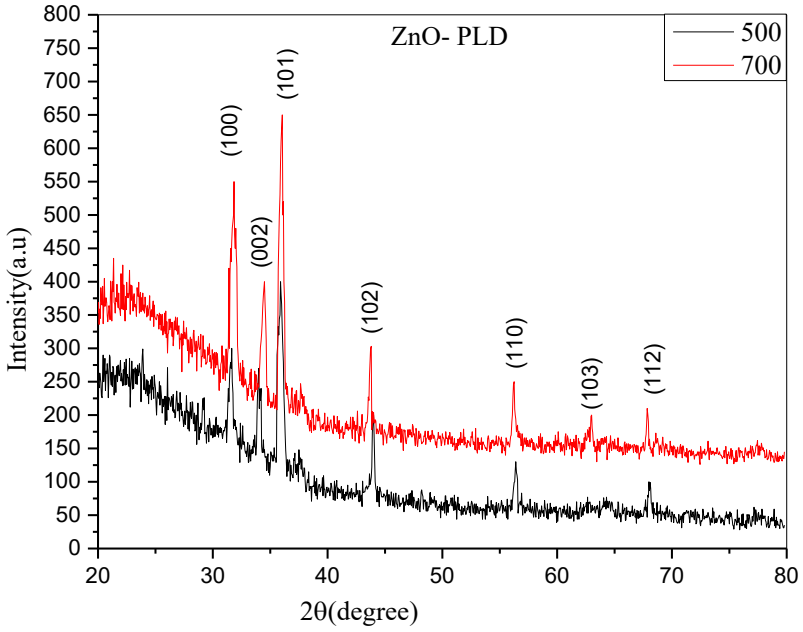

Fig. 3. XRD pattern of ZnO nanoparticles PLD.

Table 2. XRD data of ZnO nanoparticles PLD

energy	hkl	2θ (Deg.)	FWHM (Deg.)	dhkl Exp.(Å)	C.S (nm)
700	100	31.80	0.66	2.81	12.52
	002	34.40	0.63	2.60	13.20
	101	36.06	0.53	2.49	15.76
	102	43.70	0.31	2.07	27.61
	110	56.10	0.37	1.64	24.33
	103	63.05	0.28	1.47	33.28
	112	67.80	0.26	1.38	36.81
500	100	31.90	0.91	2.80	9.08
	002	34.00	0.48	2.63	17.31
	101	35.88	0.65	2.50	12.85
	102	44.00	0.30	2.06	28.56
	110	56.47	0.42	1.63	21.47
	103	62.67	1.33	1.48	6.99
	112	68.04	0.38	1.38	25.22

Calculations of the crystallite size revealed values of approximately 17.5 nm at 500 mJ and 23.4 nm at 700 mJ (Table 2) demonstrating that increasing the laser energy leads to larger crystal growth and improved crystallinity, which is consistent with previous findings in the literature [15,17,21].

XRD analysis of iron oxide nanoparticles synthesized by pulsed laser ablation at different temperatures 500 and 700 mJ indicates that the sample synthesized at 500 mJ has broad peaks and low intensity with higher values of FWHM show in Fig. 4. This shows reduced crystallite sizes, 5 to 24 nm in size and a relatively low level of crystallinity. In contrast, the samples prepared at 700 mJ showed sharper and more intense peaks with smaller FWHM values, reflecting significant crystal growth, an increase in crystallite size to approximately 44 nm, and improved crystallinity, as shown in Table 3. The smaller crystallite size at 500 mJ results in a larger surface area and more crystal defects, thus increasing the chemical activity of the material. Conversely, increasing the

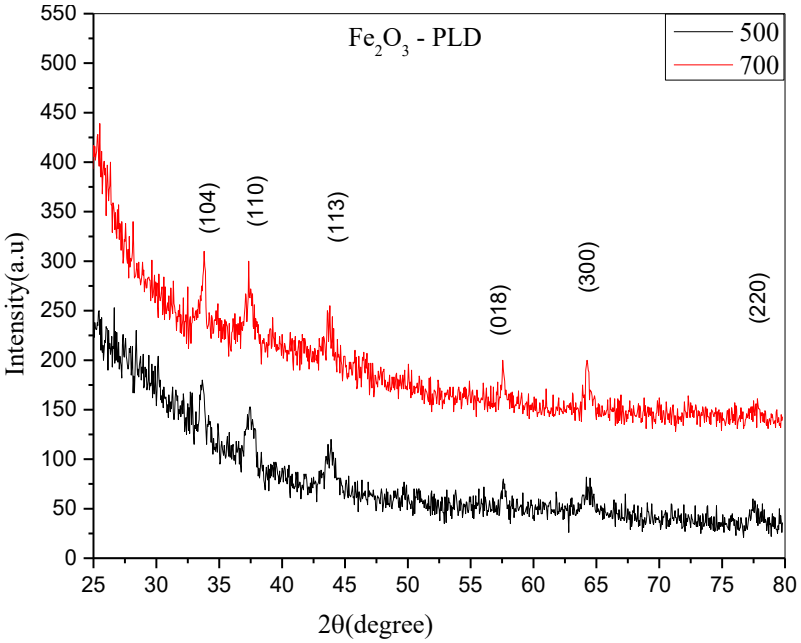

Fig. 4. XRD pattern of Fe_2O_3 nanoparticles PLD.

Table 3. XRD data of Fe_2O_3 nanoparticles PLD.

energy	hkl	2θ (Deg.)	FWHM (Deg.)	dhkl Exp.(Å)	C.S (nm)
500	104	33.69	1.62	2.66	5.12
	110	37.40	1.34	2.40	6.26
	113	43.78	1.22	2.07	7.02
	018	57.57	0.57	1.60	15.90
	300	64.38	1.07	1.45	8.77
	220	77.49	0.42	1.23	24.25
700	104	33.80	2.39	2.65	3.47
	110	37.35	1.59	2.41	5.27
	113	43.80	1.42	2.07	6.03
	018	57.55	0.50	1.60	18.13
	300	64.35	0.32	1.45	29.33
	220	77.50	0.23	1.23	44.29

temperature promotes crystal growth, reduces grain boundaries and defects, and improves crystallinity at the expense of a reduced specific surface area [16,18].

Morphology analysis using FE-SEM

The surface morphology and grain size distribution of the deposited thin films were studied using the field emission scanning electron microscopy (FE-SEM). Fig. 5 represents the scanning electron microscope (FE-SEM) images of (NiO) nanoparticles prepared by the method of PLD at a wavelength of 500 and 700 nm. The shape of the particles is almost spherical with a certain level of agglomeration of the particles attributed to the close contact of the particles. The particles at 500 mJ are smaller and seem to be more homogeneous and were of a size of about 44.15 nm on average. The particles become bigger and less regular in its shape at 700 mJ and their average diameter remains at about 51.89 nm. Such difference is explained by the higher power of laser which enriches the motion of atoms on the substrate surface, providing the better opportunity of coalescence of nuclei and formation of bigger crystals. This also results in a more widely distributed size composition, as can be seen in the accompanying graphs [11, 19, 23]. The FE-SEM images shown in Fig. 6 of ZnO nanoparticles prepared by pulsed laser deposition (PLD) technique at two different energies, 700 and 500 mJ, as well as the particle size distribution plots, show that increasing the laser energy from 500 to 700 mJ resulted in an increase in the average particle size to about 23.24 nm, indicating the formation of larger particles at higher energies. Morphologically, samples prepared at 500 mJ exhibited relatively homogeneous, fine-grained spherical particles with a partially agglomerated appearance, while samples prepared at 700 mJ exhibited larger and more diverse aggregates in shape and size, indicating that increasing laser energy promotes particle growth and increases their heterogeneity. This behavior can be explained by the fact that increasing the pulse energy during the PLD process leads to an increase in the ejection rate and energy of the ejected species towards the surface, which enhances their dispersion and coalescence, resulting in larger and less homogeneous particles [14, 15, 24]. (FE-SEM)

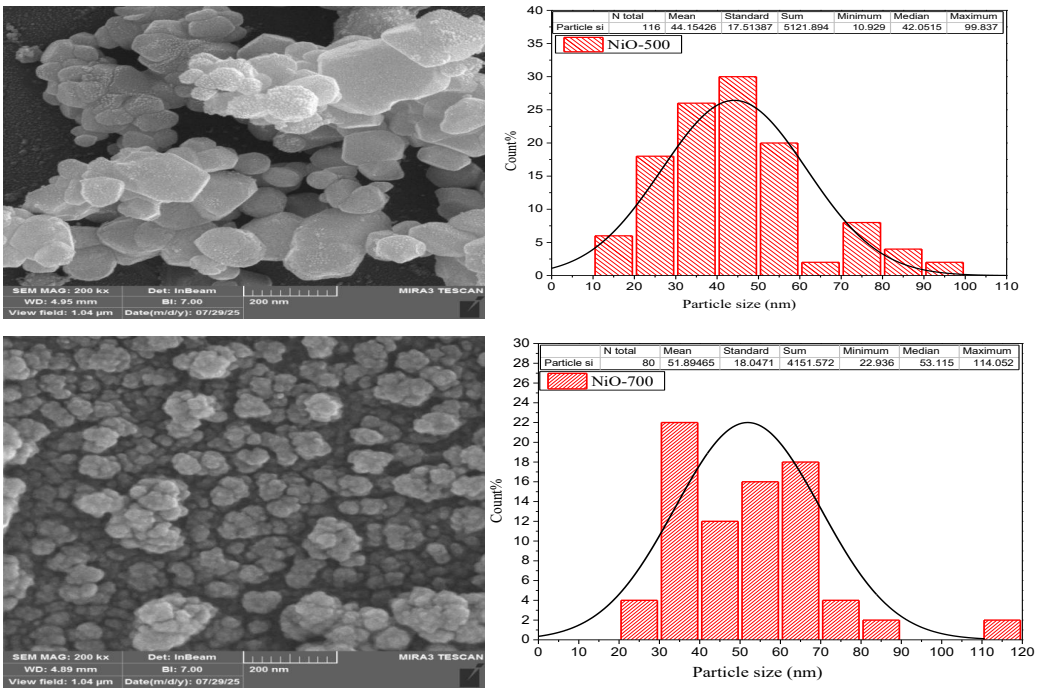

Fig. 5. Scanning electron microscope images of nickel oxide nanoparticles prepared by PLD at energies of 500 and 700 mJ, with a graph of the particle size distribution.

images and size distribution plots of iron oxide particles prepared in the same way at two different energies (500 and 700 mJ) (as shown in Fig. 7) show that laser energy clearly affects both size and shape, with the average particle size at energy 500 mJ at about 35.8 nm. The particles appeared partially clumped with irregular edges and semi-irregular shapes that tended to merge with each other, indicating inhomogeneous growth and a wide distribution in particle size. At 700 nm, the average size decreases to approximately 22.7 nm, and the particles appear more regular and closely shaped, with pronounced spherical tendencies, a more homogeneous distribution, and better surface coverage. This difference is attributed to the fact that increasing the laser power in PLD technology increases the ejection rate and the number of nucleation centers, which leads to the formation of a larger number of small, closely shaped particles, while lower energy allows for the growth of larger, less regular particles, which explains the contrast in images and histograms between the two energies [16,18,25].

DC electrical conductivity

The electrical conductivity curves of (ZnO) ,(NiO) and (Fe_2O_3) prepared by pulsed laser deposition (PLD) technique at two different energies (500 and 700 mJ) showed a distinct semiconductor behavior for all samples, (as shown in Figs. 8, 9 and 10). The electrical conductivity increased with temperature due to the activation of charge carriers (electrons or holes) and the improvement of their mobility within the crystal lattice. It was observed that the samples prepared at 700 mJ had higher conductivity than their counterparts at 500 mJ due to improved crystallinity, reduced structural defects and increased oxygen vacancies that act as electron doping centers. The 700-ZnO sample showed a clear increase in conductivity compared to the 500-ZnO sample due to fewer defects and grain boundaries [9,27]. While the 700-NiO sample showed the highest thermal response due to increased vacancy density and improved crystal order, which reduced internal resistance and facilitated charge transfer between grains [13,28]. The Fe_2O_3 sample deposited at 700 mJ showed higher conductivity due to improved crystallinity and increased oxygen vacancies compared to the 500 mJ sample. It can be concluded that increasing the preparation energy from 500 to 700 mJ improved the electrical conductivity of all oxides

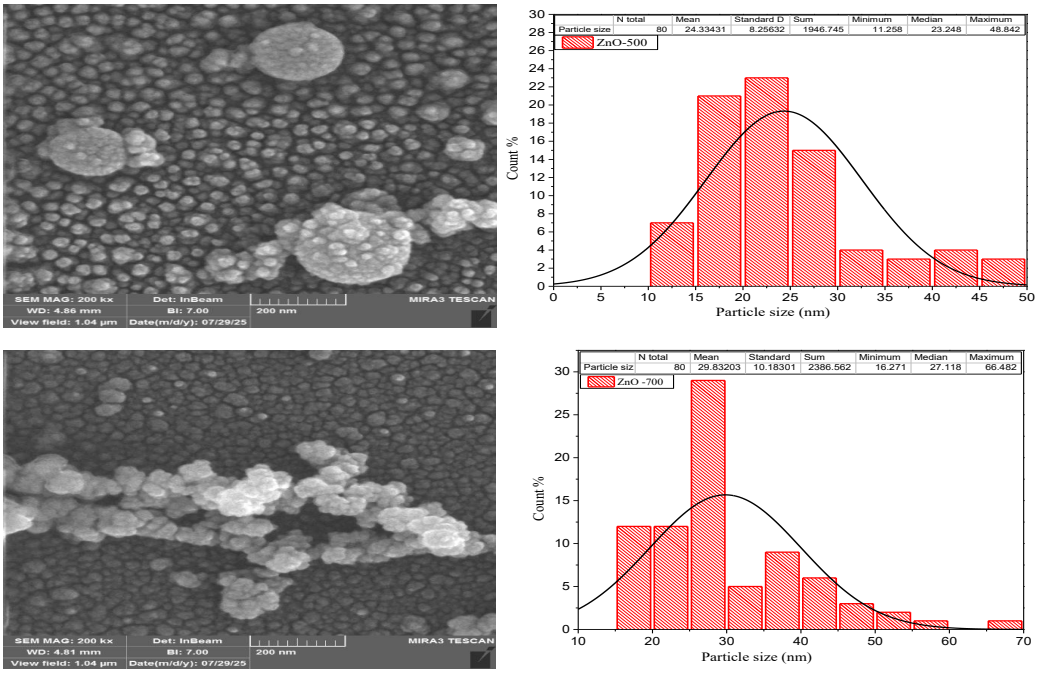

Fig. 6. Scanning electron microscope images of ZnO nanoparticles prepared by PLD at energies of 500 and 700 mJ, with a graph of the particle size distribution.

[4,26]. The three are clearly distinguished, thanks to the improvement of the crystal structure, the reduction of defects, and the increase in the number of effective charge carriers. In comparison between the materials, (NiO) showed the highest conductivity and thermal response, followed by (Fe_2O_3) and then (ZnO), which reflects the difference in charge transport mechanisms depending on the nature of each oxide and its crystal structure.

Antibacterial activity

Antibacterial activity against both Gram-negative (Escherichia coli) and Gram-positive (Staphylococcus aurous) bacteria was tested using the agar diffusion method. Zones of inhibition were measured after incubating the samples for 24 hours at 37°C. Antibacterial tests of thin films prepared by pulsed laser deposition (PLD) of ZnO, NiO, and Fe_2O_3 oxides at 500 and 700 mJ showed a significant effect against both E. coli (Gram-negative) and Staphylococcus (Gram-positive) bacteria (see Figs. 11, 12, and 13). The inhibition effect increased with increasing sample concentration from 12.5% to 100%. Increasing the laser energy from 500 to 700 mJ improved the biological activity of all samples due to the increased surface area. Zinc oxide (ZnO) showed the highest antibacterial activity compared to other oxides, due to its high production of reactive oxygen species (ROS) [22, 14, 12]. It also exhibited wide inhibition zones and strong activity, especially against E. coli, indicating its high ability to penetrate the cell wall of Gram-negative bacteria. Nickel oxide was the least effective on the list of the other oxides, and had reasonable antibacterial activity. Nevertheless, its action was stronger against Gram-positive bacteria like *Staphylococcus aureus* as opposed to its action against Gram-negative *Escherichia coli*. Its limited effectiveness is due to its weak effect at high concentrations, especially when dealing with Gram-positive strains with stronger wall structures. Based on the results, the biological activity of the studied oxides can be ranked according to their efficiency as follows: ZnO, Fe_2O_3, and NiO. It was also observed that increasing the laser energy used in the preparation from 500 to 700 mJ led to a significant improvement in the ligand capacity of these films, confirming the association between nanoscale properties and molecular structure and its direct role in antibacterial activity [10, 18, 29].Table 4 shows the antibacterial activity of Nickel oxide, Zinc oxide, and Iron oxide nanoparticles prepared

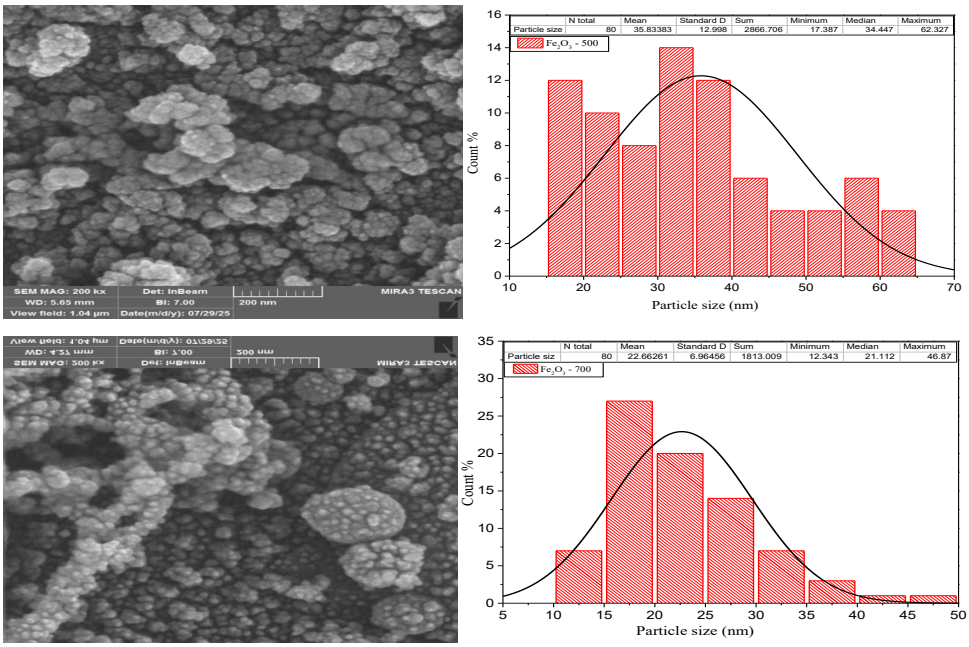

Fig. 7. Scanning electron microscope images of Fe_2O_3 nanoparticles prepared by PLD at energies of 500 and 700 mJ, with a graph of the particle size distribution.

using PLD at two different energies, 700 and 500, against Staphylococcus aurous and Escherichia coli, the inhibition zone was measured in millimeters at different concentrations (A constant group, B 2.5%, C 25%, D 50%, E 100%). It is clear that the Zinc oxide nanoparticle sample at 700 PLD showed the largest inhibition zones against bacteria (up to 30-32 mm against S. aurous and 24-25 mm against E. coli), indicating the powerful effect of (ZnO), especially at high energies. On the other hand, (NiO) particles showed relatively less inhibition, with maximum values of 22-24 mm against S. aurous and 18-21 mm against E. coli. Fe_2O_3 showed intermediate activity, achieving concentrations of 27-28 mm against S. aurous and 20-24 mm against E. coli. Overall, the response was stronger against S. aurous (Gram-positive bacteria) than against E. coli (Gram-negative bacteria). (Gram), and increasing the concentration (from A to E) and increasing the preparation energy led to enhanced

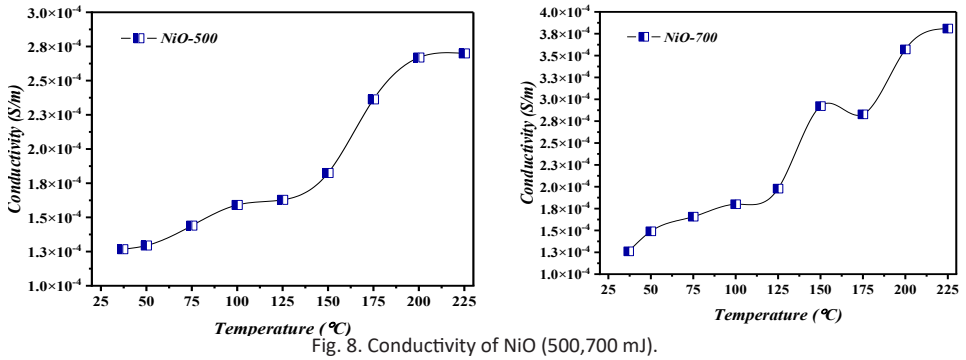

Fig. 8. Conductivity of NiO (500,700 mJ).

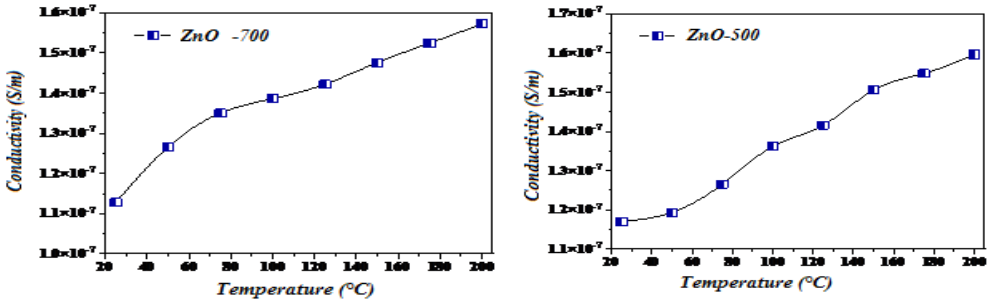

Fig. 9. Conductivity of ZnO (500,700 mJ).

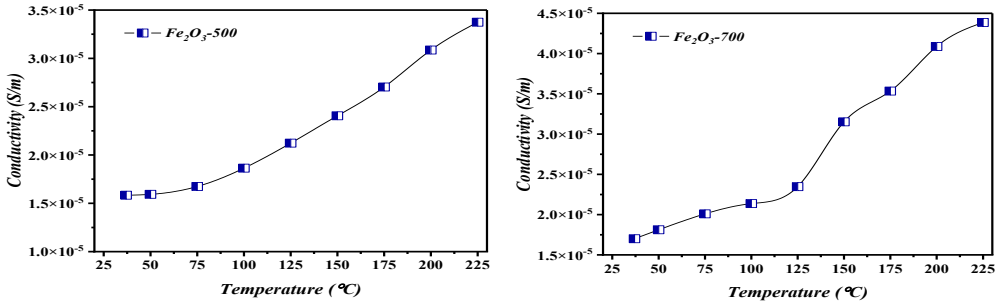

Fig. 10. Conductivity of Fe_2O_3 (500,700 mJ).

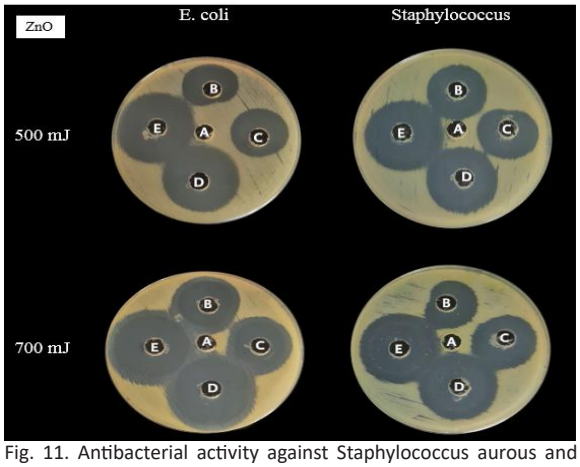

Fig. 11. Antibacterial activity against Staphylococcus aurous and Escherichia coli using PLD-prepared ZnO nanoparticles. A: Control group. B: 12.5%. C: 25%. D: 50%. E: 100%.

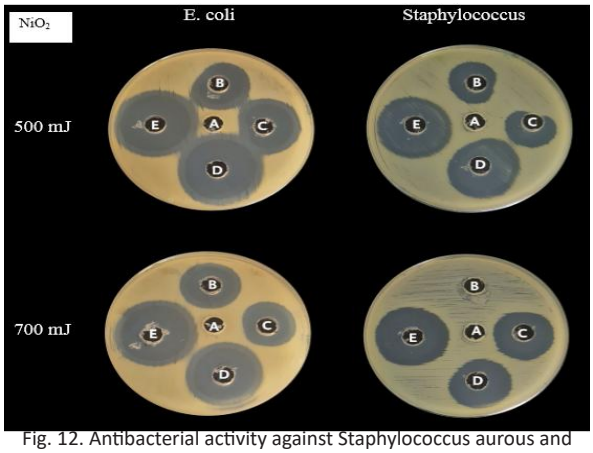

Fig. 12. Antibacterial activity against Staphylococcus aurous and Escherichia coli using PLD-prepared NiO_2 nanoparticles. A: Control group. B: 12.5%. C: 25%. D: 50%. E: 100

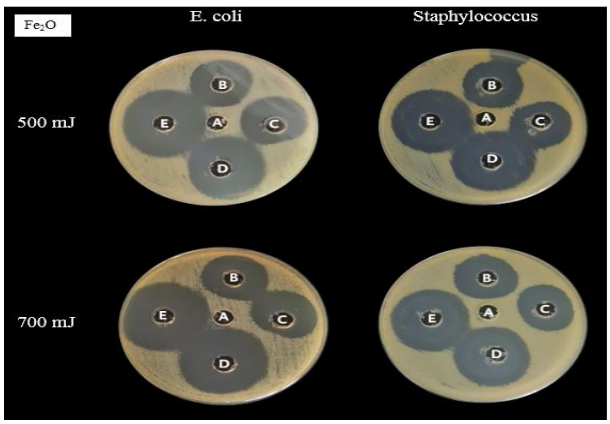

Fig. 13. Antibacterial activity against Staphylococcus aurous and Escherichia coli using PLD-prepared Fe_2O_3 nanoparticles. A: Control group. B: 12.5%. C: 25%. D: 50%. E: 100%.

Table 4. Explain the antibacterial activity of nanoparticles.

sample		A	B	C	D	E
S.aureus	NiO NPs 700 PLD	6	17	18	22	23
E.coli		6	6	17	18	20
S.aureus	NiO NPs 500 PLD	6	18	19	23	24
E.coli		6	15	16	19	21
S.aureus	ZnO NPs 700 PLD	6	19	20	30	32
E.coli		6	16	19	24	25
S.aureus	ZnO NPs 500 PLD	6	16	17	23	24
E.coli		6	17	18	22	23
S.aureus	Fe_2O_3 NPs 700 PLD	6	18	19	27	28
E.coli		6	14	15	20	22
S.aureus	Fe_2O_3 NPs 500 PLD	6	18	19	22	25
E.coli		6	16	17	23	24

antibacterial activity, which was associated with an increase in the size of the inhibition zone [30,31].

CONCLUSION

Zinc, nickel, and iron oxide films were prepared by pulsed laser deposition (PLD) at two energy levels (500 and 700 mJ). The results showed that increasing the laser energy improved the structural, morphological, conductive, and biological properties. XRD examinations showed that the samples were crystalline pure, with improved crystallinity as the energy increased, with a clear increase in the crystallite size of ZnO and Fe_2O_3, and a slight decrease in NiO. FE-SEM images showed tightly packed spherical particles, the size of which was affected by increasing energy. The electrical conductivity of all samples increased with temperature and power, and was highest for NiO, followed by Fe_2O_3 and then ZnO.

ZnO showed the highest antibacterial activity followed by Fe_2O_3 and NiO, with increased efficacy at higher energy levels. The results confirm that the improvement of the crystal structure resulting from the increase in laser energy enhances the electrical and biological performance of these oxides, making them suitable for bioelectronics and antibacterial applications.

CONFLICT OF INTEREST

The authors declare that there is no conflict of interests regarding the publication of this manuscript.

REFERENCES

1. Tsuda N, Nasu K, Fujimori A, Siratori K. Representative Conducting Oxides. Springer Series in Solid-State Sciences: Springer Berlin Heidelberg; 2000. p. 157-319.
2. Jüngel A, Pinnau R, Röhrig E. Analysis of a bipolar energy-transport model for a metal-oxide-semiconductor diode. Journal of Mathematical Analysis and Applications. 2011;378(2):764-774.
3. Krebs H-U, Weisheit M, Faupel J, Süske E, Scharf T, Fuhse C, et al. Pulsed Laser Deposition (PLD) A Versatile Thin Film Technique. Advances in Solid State Physics: Springer Berlin Heidelberg; 2003. p. 505-518.
4. Jihad GH. Synthesis and Characterization of α-Fe_2O_3 Nanoparticles Prepared by PLD at Different Laser Energies. Iraqi Journal of Science. 2021:3901-3910.
5. Kadhim FJ, Bedoui MH. Copper Oxide Nanoparticles (CuO NPs) prepared from Chitosan extract for antibacterial activity. Research Square Platform LLC; 2024.
6. Abbas Khudhir I, Essa AF. Preparation and characterization of polypyrrole/ carbon nanotube composites using ZnO, MgO and MnO. Journal of Physics: Conference Series. 2025;2974(1):012029.
7. Naser DK, Abbas AK, Aadim KA. Zeta Potential of Ag, Cu, ZnO, CdO and Sn Nanoparticles Prepared by Pulse Laser Ablation in Liquid Environment. Iraqi Journal of Science. 2020:2570-2581.
8. Najim AA, Hassan FM, Rasheed HS, Ismail H, Darwoysh HH. Experimental investigation to determine the optical properties of $(Fe_2O_3)_{1-x}(NiO)_x$ thin films prepared by PLD technique for NLO applications. Opt Mater. 2021;121:111602.

9. Al-Assiri MS, Mostafa MM, Ali MA, El-Desoky MM. Synthesis, structural and electrical properties of annealed ZnO thin films deposited by pulsed laser deposition (PLD). Superlattices Microstruct. 2014;75:127-135.
10. Suturin SM, Korovin AM, Sitnikova AA, Kirilenko DA, Volkov MP, Dvortsova PA, et al. Correlation between crystal structure and magnetism in PLD grown epitaxial films of ε-Fe_2O_3 on GaN. Science and Technology of Advanced Materials. 2021;22(1):85-99.
11. Shkir M, Khan A, Chandekar KV, Sayed MA, El-Toni AM, Ansari AA, et al. Dielectric and electrical properties of La@ NiO SNPs for high-performance optoelectronic applications. Ceram Int. 2021;47(11):15611-15621.
12. Olteanu A-M, Nicoara A-I, Surdu V-A, Isopencu G-O, Banciu D-D, Jinga S-I, et al. Antibacterial activity of tin-doped zinc oxide thin films deposited by laser ablation. Ceram Int. 2024;50(2):3497-3510.
13. Liu M, Wang Y, Li P, Cheng Z, Zhang Y, Zhang M, et al. Preparation and characterization of multilayer NiO nano-products via electrospinning. Appl Surf Sci. 2013;284:453-458.
14. Puspasari V, Ridhova A, Hermawan A, Amal MI, Khan MM. ZnO-based antimicrobial coatings for biomedical applications. Bioprocess and Biosystems Engineering. 2022;45(9):1421-1445.
15. Study of Gallium-Doped Zinc Oxide Thin Films Processed by Atomic Layer Deposition and RF Magnetron Sputtering for Transparent Antenna Applications. American Chemical Society (ACS).
16. Teng X, Qin Y, Wang X, Li H, Shang X, Fan S, et al. A Nanocrystalline Fe_2O_3 Film Anode Prepared by Pulsed Laser Deposition for Lithium-Ion Batteries. Nanoscale Research Letters. 2018;13(1).
17. Mahmoudi Khatir N, Khorsand Zak A. Antibacterial activity and structural properties of gelatin-based sol-gel synthesized Cu-doped ZnO nanoparticles; promising material for biomedical applications. Heliyon. 2024;10(17):e37022.
18. Khamees EJ, Saeed IA, Abdulazeem L, Gençyılmaz O, Agarwal MK, Mohammed KA, et al. Generation and Investigation of FE2O3 Nanoparticles' Optical Properties and Antibacterial Activity Using Pulsed Laser Ablation in Deionized Water. International Journal of Nanoscience. 2023;23(02).
19. Qiu Z, Gong H, Zheng G, Yuan S, Zhang H, Zhu X, et al. Enhanced physical properties of pulsed laser deposited NiO films via annealing and lithium doping for improving perovskite solar cell efficiency. Journal of Materials Chemistry C. 2017;5(28):7084-7094.
20. Keraudy J, García Molleja J, Ferrec A, Corraze B, Richard-Plouet M, Goullet A, et al. Structural, morphological and electrical properties of nickel oxide thin films deposited by reactive sputtering. Appl Surf Sci. 2015;357:838-844.
21. Negi A, Ringwal S, Pandey M, Taha Yassin M. Plant-mediated Z-scheme ZnO/TiO2-NCs for antibacterial potential and dye degradation: experimental and DFT study. Sci Rep. 2024;14(1).
22. El-Habib I, Maatouk H, Lemarchand A, Dine S, Roynette A, Mielcarek C, et al. Antibacterial Size Effect of ZnO Nanoparticles and Their Role as Additives in Emulsion Waterborne Paint. Journal of Functional Biomaterials. 2024;15(7):195.
23. Khan A, Shkir M, Ansari SA, Parveen N, AlFaify S, El-Toni AM, et al. One-pot flash combustion synthesis of Fe@NiO nanocomposites for supercapacitor applications. Ceram Int. 2021;47(7):9024-9033.
24. Venkatachalam S, Iida Y, Kanno Y. Preparation and characterization of Al doped ZnO thin films by PLD. Superlattices Microstruct. 2008;44(1):127-135.
25. Hasan SJ, Evan TS, Rana OM, Iman HH, Subash CBG. A Study on Different Au Concentrations for A-Fe_2O_3@Au Hybrid Structure Preparation and Characterization. International Journal of Nanoelectronics and Materials (IJNeaM). 2025;18(June):139-152.
26. Cao J, Kako T, Kikugawa N, Ye J. Photoanodic properties of pulsed-laser-deposited α-Fe_2O_3 electrode. J Phys D: Appl Phys. 2010;43(32):325101.
27. Das AK, Misra P, Kumar R, Ganguli T, Singh MK, Phase DM, et al. Studies on highly resistive ZnO thin films grown by DC-discharge-assisted pulsed laser deposition. Appl Phys A. 2013;114(4):1119-1128.
28. Zhang L, Liu W, Wen X, Chen J, Zhao C, Castillo-Rodríguez M, et al. Electrospun submicron NiO fibers combined with nanosized carbon black as reinforcement for multi-functional poly(lactic acid) composites. Composites Part A: Applied Science and Manufacturing. 2020;129:105662.
29. Giedraitienė A, Ružauskas M, Šiugždinienė R, Tučkutė S, Grigonis K, Milčius D. Development of Antibacterial Cotton Textiles by Deposition of Fe_2O_3 Nanoparticles Using Low-Temperature Plasma Sputtering. Nanomaterials. 2023;13(24):3106.
30. Mostafa AM, Mwafy EA. The effect of laser fluence for enhancing the antibacterial activity of NiO nanoparticles by pulsed laser ablation in liquid media. Environmental Nanotechnology, Monitoring and Management. 2020;14:100382.
31. Khashan KS, Sulaiman GM, Hamad AH, Abdulameer FA, Hadi A. Generation of NiO nanoparticles via pulsed laser ablation in deionised water and their antibacterial activity. Appl Phys A. 2017;123(3).